J Mater Sci: Mater Electron (2021) 32:3948–3957

Effects of Cu doping on the structural, photoluminescence and impedance spectroscopy of CoS_2 thin films

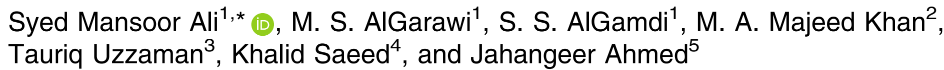

Syed Mansoor Ali[1,*], M. S. AlGarawi[1], S. S. AlGamdi[1], M. A. Majeed Khan[2], Tauriq Uzzaman[3], Khalid Saeed[4], and Jahangeer Ahmed[5]

[1] *Department of Physics and Astronomy, College of Science, King Saud University, P.O. Box 2455, Riyadh 11451, Saudi Arabia*
[2] *King Abdullah Institute for Nanotechnology, King Saud University, Riyadh 11451, Saudi Arabia*
[3] *Electrical Engineering Department, College of Engineering, King Saud University, Riyadh, Saudi Arabia*
[4] *Engineering Research Institute, Ulster University, Jordanstown, Newtownabbey BT37 0QB, Co. Antrim, UK*
[5] *Department of Chemistry, College of Science, King Saud University, P.O. Box 2455, Riyadh 11451, Saudi Arabia*

Received: 28 September 2020
Accepted: 16 December 2020
Published online:
5 January 2021

© The Author(s), under exclusive licence to Springer Science+Business Media, LLC part of Springer Nature 2021

ABSTRACT

Copper-doped cobalt sulfide ($Cu_xCo_{1-x}S_2$: x = 0–0.1) nanocrystalline thin films were deposited on glass substrates using successive ionic layer adsorption and reaction (SILAR) technique. The influence Cu element concentration on nanostructural, morphological, photoluminescence and impedance properties of $Cu_xCo_{1-x}S_2$ thin films were examined by means of X-ray diffraction (XRD), field emission scanning electron microscopy (FESEM), electron dispersive X-ray (EDX) photoluminescence (PL) and impedance spectroscopy. XRD results revealed that all prepared films consist of pure cubic phase of CoS_2 pyrites structure and were well crystallized with the preferentially oriented along (200) plane. Cu doping resulted in a significant increase in the crystallinity of the films and a noticeably alteration in crystallite size. FESEM images revealed that the deposited thin film having spherical grain distribution and the grain sizes decreased from 56 to 34 nm with increasing Cu doping level. The EDX analysis confirmed the stoichiometry of prepared thin films. Photoluminescence (PL) spectra display the broad emission bands centered at 411 with a hump at 417 nm, due to the intrinsic defects. From the impedance spectroscopy analysis, we examined the equivalent circuit and frequency-dependent relaxation phenomenon in dielectric dipoles, loss of electrical energy and AC conductivity of the pure and Cu-doped thin films. Finally, all properties have been discussed, as an impartial of the research work, in terms of the Cu doping content.

Address correspondence to E-mail: mansoor_phys@yahoo.com; symali@ksu.edu.sa

https://doi.org/10.1007/s10854-020-05136-2

1 Introduction

The transition metal dichalcogenides with pyrite structural phase such as MX_2 (M = Fe, Co, or Ni and X = S or Se) have rarely been studied in past [1]. They are of specific notice due to their tremendously low cost and predictable long term stability in the electrocatalyst and solar cell applications [2]. Recently, the interest in pyrite phase materials for advance applications has increased meaningfully due of its nontoxicity and earth-abundancy [3, 4]. Among these pyrite structural phases, cobalt pyrite (cobalt disulfide, CoS_2) fundamentally have good conductivity as compared to the other pyrites, such as NiS_2 [5] and FeS_2 [6] creating it exceptionally advantaged. The CoS_2 has a pyrites cubic structure having four Co and eight S atoms [7, 8]. It has recently fascinated and got a significant consideration for the magnetic and electrochemical characteristics for application of in spin-electronic [9], supercapacitors [10], lithium ion batteries [11], electrocatalysts activity [12] and hydrogen evolution reaction [2]. On the other hand, CoS_2 has a much high electronic conductivity, large thermal stability and is not sensitive to oxygen which makes it suitable for advanced applications.

The metal doping approach is an effective way to modify the surface state, carrier concentration or transportation and defects level in the host materials. CoS_2 thin films are doped or co-doped with numerous elements like N, P co-doped [13], N [14], Ni [15], and Mn [16]. The metal doping such as Cu are behaving as a fast-diffusing impurities in the host materials [17]. The Cu doping into CoS_2 can induced effects on its nanostructural, morphological, luminescence and electrical characteristics.

As for the deposition of CoS_2 thin films, a diversity of techniques has been studied such as solvothermal/hydrothermal [18, 19], atmospheric-pressure chemical vapor deposition [20], magnetron sputtering [21] and sulfurization of Co films [22]. In the present research, we reported a simple method to deposited single phase and crystalline with suitable composition pyrite (CoS_2) thin films via successive ionic layer adsorption and reaction (SILAR) technique. As a non-vacuum techniques, SILAR is simple, cheap and appropriate for large scale deposition with controllable thickness precise stoichiometry and dense mirror like surface morphology [23, 24]. Up to now, no one reported the preparation of CoS_2 films using SILAR method.

In the present work, for the first time, it was achieved Cu-doped CoS_2 thin film deposited with the SILAR technique. The objective is to determine the nanostructural, morphological, photoluminescence and impedance properties of $Cu_xCo_{1-x}S_2$ thin films by increasing the Cu doping level. To find the enhancement of the nanostructure and morphological properties, the XRD and FESEM results were performed, photoluminescence spectra were carried out to investigate the intrinsic emission with effect of Cu doping and impedance analysis were obtained to determine the capacitance and resistance of grain and grain boundaries of the prepared thin films. whether the bandgap value decreased and increased. The effect of Cu doping that is critical for tuning the properties of CoS_2 thin films have been studied.

2 Experimental

Pure and Cu-doped CoS_2 thin film was deposited using SILAR method. Prior to the thin films deposition, glass substrates were ultrasonically washed with ethanol and deionized water for 15 min. The solutions of 0.25 M $Co(NO_3)_2$ with adding of different contents (0 to 10%) of $Cu(NO_3)_2$ for Cu content according to doping level in deionized water for cations solution. Second solution of 0.25 M Na_2S aqueous solution was used as anions sources solutions. The preparation of thin films was carried in four steps to complete one SILAR cycle: First, immersed in cations solution for 2 min to adsorption of cations; second, dried and rinsed with deionized water; third, immersed in anions solution for 2 min to reaction of anions with pre-adsorbed cations and fourth, dried and rinsed with deionized water. To obtain pure and Cu-doped CoS_2 thin films with appropriate thickness, the 30 SILAR cycles were performed.

The prepared thin films were structurally characterized by X-ray diffraction (XRD) analysis using a Panalytical X'Pert^3 equipped with a CuKα X-ray. The surface morphology of prepared $Cu_xCo_{1-x}S_2$ thin films was performed using a FESEM (JEOL). UV–Vis spectroscopy and bandgap investigation was executed using a V-670 UV–visible spectrophotometer (JASCO) and photoluminescence study was performed with FP-8200 spectrofluorometer (JESCO). Impedance analysis of thin films was carried out using HP4294 impedance analyzer.

3 Results and discussion

Figure 1 illustrates the XRD patterns of pure and Cu-doped CoS_2 thin films with different concentrations. It can be seen that four diffraction peaks are detected for CoS_2 with indexed (111), (200), (210) and (211) at position 29.45°, 31.97°, 35.64° and 39.80°, respectively. The peak (200) is the most intensive as compared to other peaks, which specifies the preferred growth direction. The diffraction peaks confirmed the cubic phase of CoS_2 (JCPDS Card No. 65-3322). The examined results are well agreed with XRD of CoS_2 thin films reported previously [25]. It is observed that the intensity of XRD peaks rises with Cu doping, this is the indication of enhancement in crystalline nature of CoS_2 thin films.

XRD results were examined by the Rietveld refinement method using the High Score plus program as revealed in Fig. 2a–d. Table 1 illustrates of goodness of fit (χ) varies in the range of 3.23and 3.64 for pure and Cu-doped CoS_2, which is the indication of goodness of refinement. Rietveld refinements for all samples have the quality parameters (R-factors) specify a good agreed and confirming the formation of single CoS_2 phase.

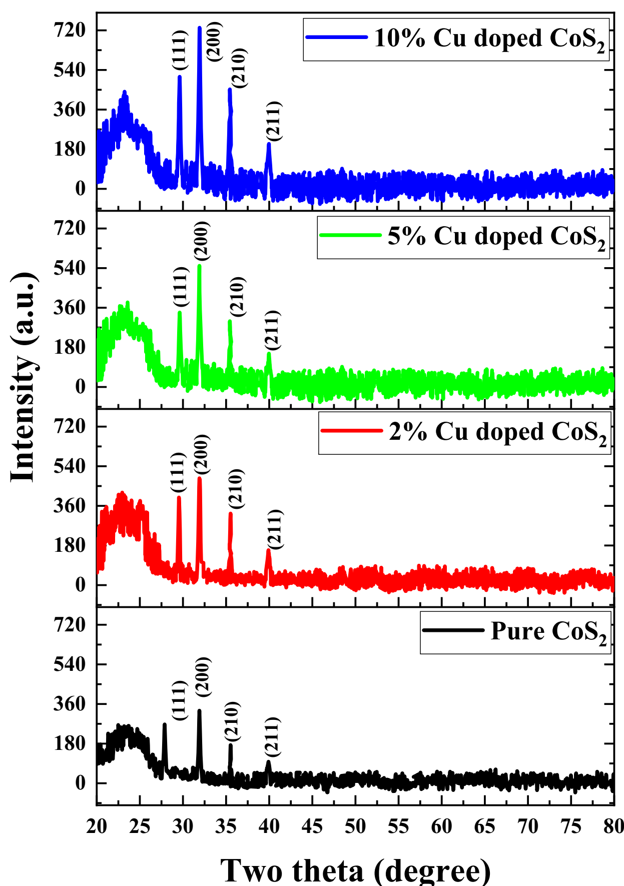

Fig. 1 X-ray diffraction patterns of $Cu_xCo_{1-x}S_2$ (x = 0–0.10) thin films in the range of 20°–80°

The Scherrer's formula is used to estimate the crystallite size (D) of pure and doped CoS_2 thin films using (200) plane.

$$D = \frac{0.9\lambda}{\beta\cos\theta} \quad (1)$$

where λ is wavelength of X-ray (λ = 1.54 Å), β is full width at half maxima (FWHM) and θ is the Bragg's angle for preferred peak. The calculated crystallite size is given in Table 1. It recognized that the crystallite size decreased with increasing the Cu doping level. This may be due to the lattice distortion caused by radius difference between the dopant and the host element. The lattice constant of the cubic phase CoS_2 is calculated using Miller indices of (200) plane [26]:

$$a = d\left(h^2 + k^2 + l^2\right)^{1/2} \quad (2)$$

where 'a' is the lattice constant, (h, k, l) are miller indices and d is the plane spacing. Variation of the prepared samples lattice constant values from the bulk material (a_0 = 5.506 Å) demonstrate that the deposited pure and Cu-doped CoS_2 thin films were under strain. The microstrain in as pure and Cu-doped thin films were calculated using the following relation [27]:

$$\varepsilon = \frac{\beta}{4\tan\theta} \quad (3)$$

The increase in the value of microstrain is due to the decrease in the crystallite size, that may have induced lattice imperfection in the CoS_2 structure. Table 1 shows the deviance of microstrain with Cu doping. The increased of micro strain is responsible for increasing the peaks intensity of XRD [28]. The dislocation density (δ) was calculated by following relation [29]:

$$\delta = \frac{1}{D^2} \quad (4)$$

It noticed that the calculated values of dislocation density increased for doped sample as compared to pure CoS_2 thin films. The lowest value of dislocation density is found for 50 kGy gamma dose with smaller crystalline size. The number of crystallites (N) per unit area and crystallite density (ρ) of prepared thin films was estimated by following relations [30]:

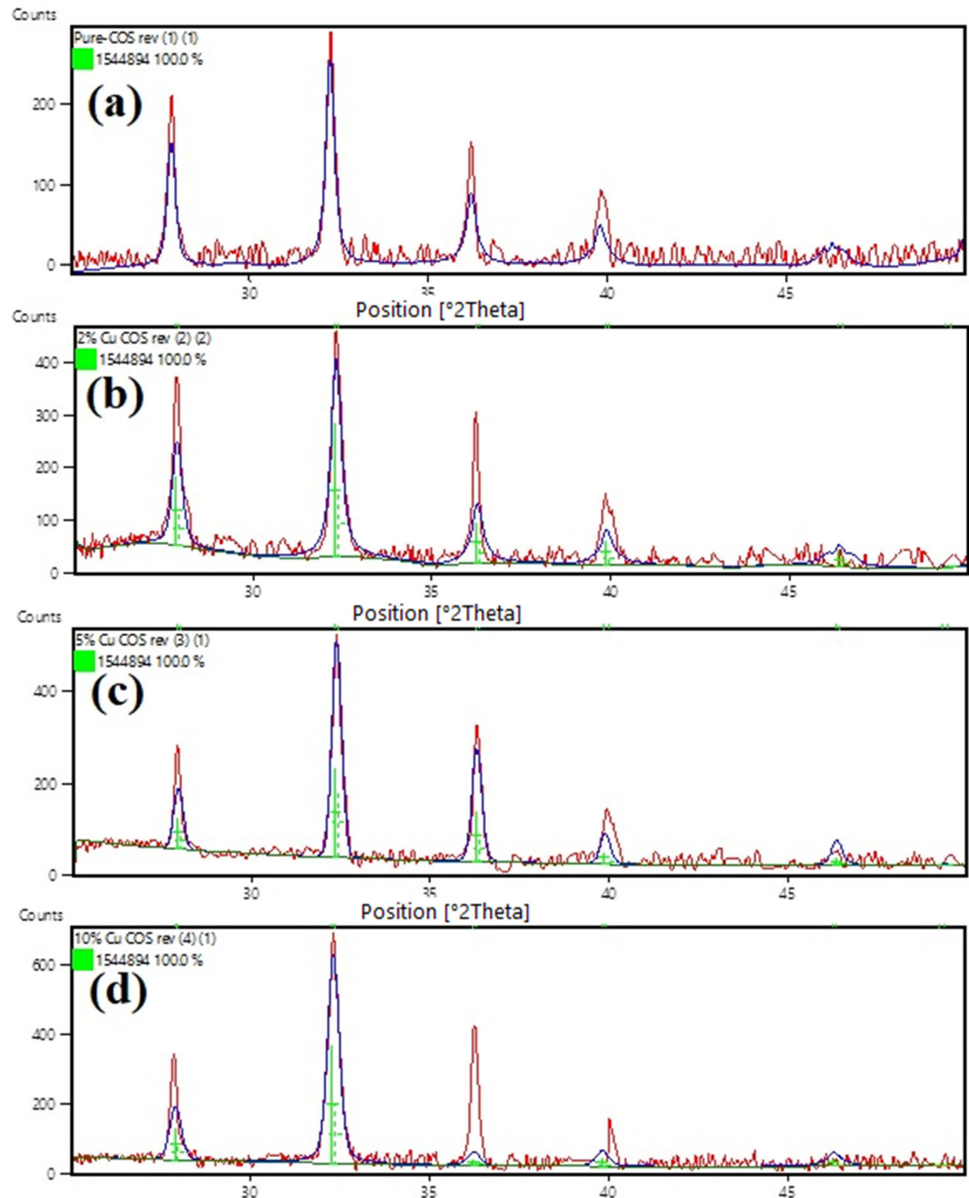

Fig. 2 Rietveld refinement of XRD data o $Cu_xCo_{1-x}S_2$ (x = 0–0.10) thin films

$$N = \frac{t}{D^3} \quad (5)$$

$$\rho = \frac{2M}{N_A V} \quad (6)$$

where t is the thickness measured by gravimetric method, N_A is the Avogadro's number (6.02 × 10^{23}), M the molecular weight of CoS_2 (123.07 g/mole) and V the volume of the unit cell. The number of crystallites increased the values of crystallite density decreased with Cu doping and this may be due to the enhancement in the nucleation and the growth of crystallites, which reasons a reduction in crystallite size and in surface area. The specific surface area S of prepared sample was calculated by following relation:

$$S = \frac{6000}{\rho \times D} \quad (7)$$

The above relation is considered for spherical shape particles as observed in the deposited thin film. The lesser specific area detected for greater crystallite size, due to the lower microstrain produced.

The field emission scanning electron micrograph of a pure and Cu-doped CoS_2 thin film of about is shown in Fig. 3a–d. The surface of the substrate was observed to be well covered with the deposited thin

Table 1 Structural parameters of $Cu_xCo_{1-x}S_2$ (x = 0–0.10) thin films

Cu doping (%)	Thickness (nm)	2θ (degree)	β (rad.)	d (Å)	a (Å)	V (Å)^3	D (nm)	$\varepsilon \times 10^{-3}$	δ (1/nm^2) $\times 10^{-3}$	$N \times 10^{15}$	ρ (g/cm^3)	S (cm^2/g)	R-Factor	χ
0	263	31.939	0.0051	2.809	5.617	177.22	28.27	4.46	1.25	8.85	2.31	91.87	15.29	3.23
2	254	31.936	0.0063	2.782	5.564	172.25	22.83	5.50	1.91	16.8	2.37	110.89	17.17	3.46
5	271	31.935	0.0069	2.777	5.553	171.23	20.89	6.03	2.29	21.9	2.39	120.17	16.94	3.53
10	265	31.934	0.0071	2.769	5.546	170.58	20.30	6.20	2.42	23.9	2.40	123.15	18.52	3.35

film, having spherical grain distribution. The observed average grain sizes decreased were between 61 and 38 nm with increasing the Cu concentration. Surface morphology of CoS_2 deposited shows that the small grains agglomerated and form the cluster of particles, the size of cluster is increased as the Cu doping concentration increases.

The EDX analysis of $Cu_xCo_{1-x}S_2$ (x = 0–0.1) is depicted in Fig. 4a–d, to confirm the stoichiometry of prepared thin films. Their consequential atomic and weight percentages are revealed insets of Fig. 4a–d. In the pure thin films, the atomic percentages of Co and S were approximately 43% and 57%, respectively, which shows the deposition of CoS_2 on glass substrate. As the doping level is increased, the atomic composition of Co and S decreased. The EDX spectra confirmed the formation of $Cu_xCo_{1-x}S$ with Cu percentages.

Room temperature photoluminescence spectra of pure and Cu-doped CoS_2 thin films at excitation wavelength of 350 nm are shown in Fig. 5. It is found that prepared thin films have two fundamental peaks located at 411 nm and 417 nm. This is due to the intrinsic defects such as Co interstitials, S vacancies and Co vacancies. These defects can trap the electrons to form ionization point defects and therefore behave like radiative centers. Moreover, these traps act as donors and produce new energy level and consequential create the PL emissions [31]. The intensity of broad PL peak band modifies by Cu doping. After doping, the intensity gradually intensifies with respect to pure CoS_2 thin films. This phenomenon can be understood as it is contended in XRD analysis that Cu atoms incorporate in CoS_2 as substitutional and interstitial, respectively. That may increase the density of defects, resulting in an improvement in the peak intensity. The clear increased in the FWHM in PL peak indicates the enhancement in the crystallinity of the structure with Cu doping [32]. The blue shift in PL peak with Cu doping is attributed to electronic structure alterations in the CoS_2 thin films.

To measure the electrical properties of materials needs powerful techniques to investigate the electrical performance, which is through simulating by an equivalent circuit [32]. Impedance analysis is an appropriate procedure to examine the numerous effects of Cu doping concentration. The electrical characteristic (Nyquist plots) is shown in Fig. 6a with the presence of semicircular arcs for pure and Cu-doped CoS_2 thin films. The phenomena that occur in

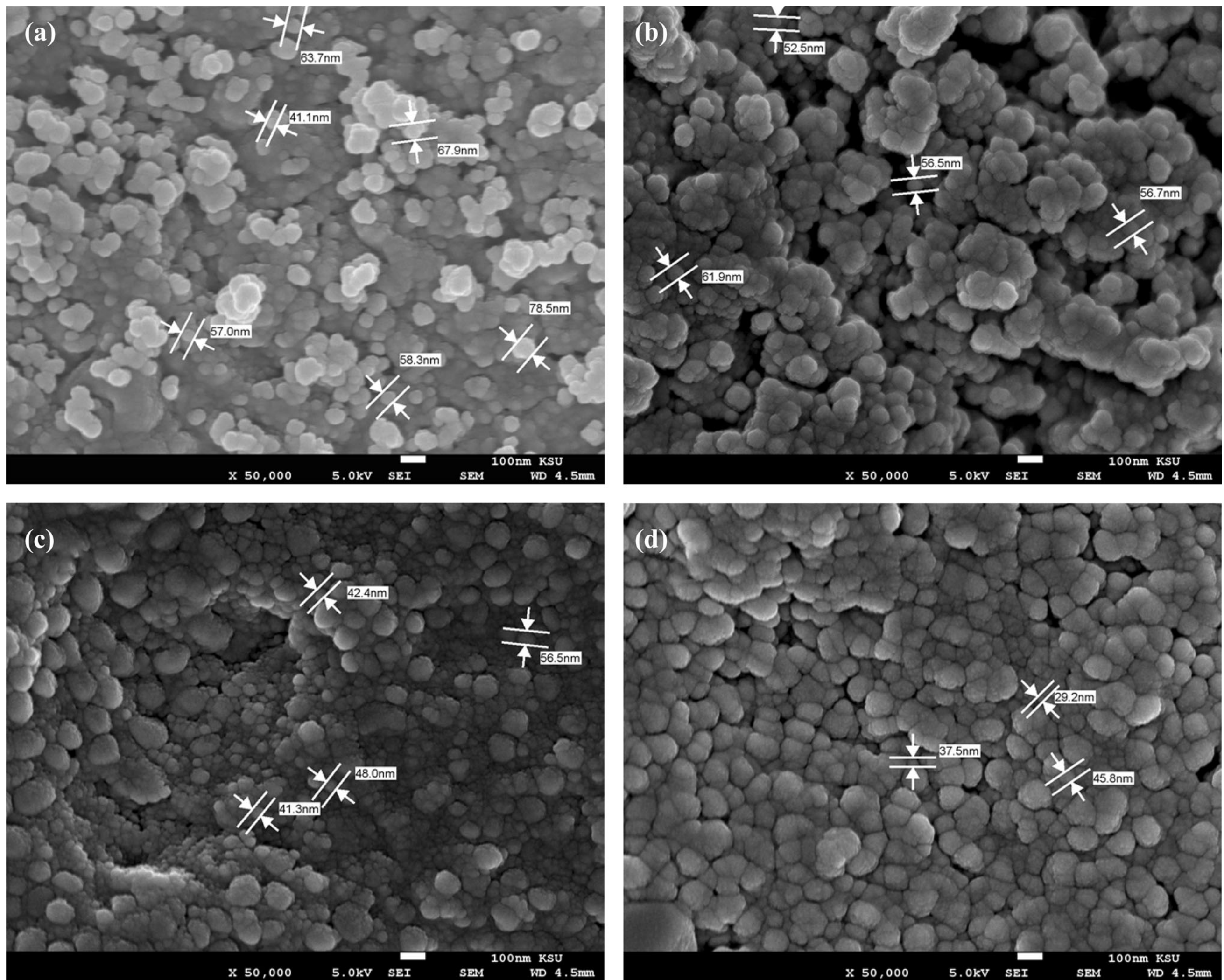

Fig. 3 **a**–**d** FESEM images of $Cu_xCo_{1-x}S_2$ (x = 0–0.10) thin films

the thin films are exhibited by an equivalent electrical circuit as shown inset of Fig. 6. The deviation of the resistance ($R1$) and capacitance ($C1$) as a function of Cu doping concentration are given in Table 2. It is noticed that the resistance of CoS_2 increases and the capacitance decreases with the increase of Cu doping concentration. For high Cu doping level, exclusion of Cu in between the interface of grain boundaries that causing an upsurge in resistance [33]. This change due to the incorporation of Cu in CoS_2 lattice that induces changes in the grain size and therefore generates extra grain boundaries within thin films [34]. There are two mechanisms that are simultaneously present, charge transformation across the grain and grain boundaries due to the increase of grain boundaries with Cu doping concentration.

To investigate the dielectric properties of pure and Cu-doped CoS_2 thin films for appreciated study about electric polarization and conduction mechanisms [35]. It is significant to note that permittivity and permeability of materials are not same. These can have modified with applied frequency, nanostructure and temperature of material [36]. The values of real and imaginary dielectric constant and dielectric loss ($\tan\delta$) were computed from impedance analysis data using following equations [37]:

$$\varepsilon' = \frac{t}{fA\epsilon_0} \cdot \frac{Z''}{Z'^2 + Z''^2} \tag{8}$$

$$\varepsilon'' = \frac{t}{fA\epsilon_0} \cdot \frac{Z'}{Z'^2 + Z''^2} \tag{9}$$

$$\tan\delta = \frac{\varepsilon''}{\varepsilon'} \tag{10}$$

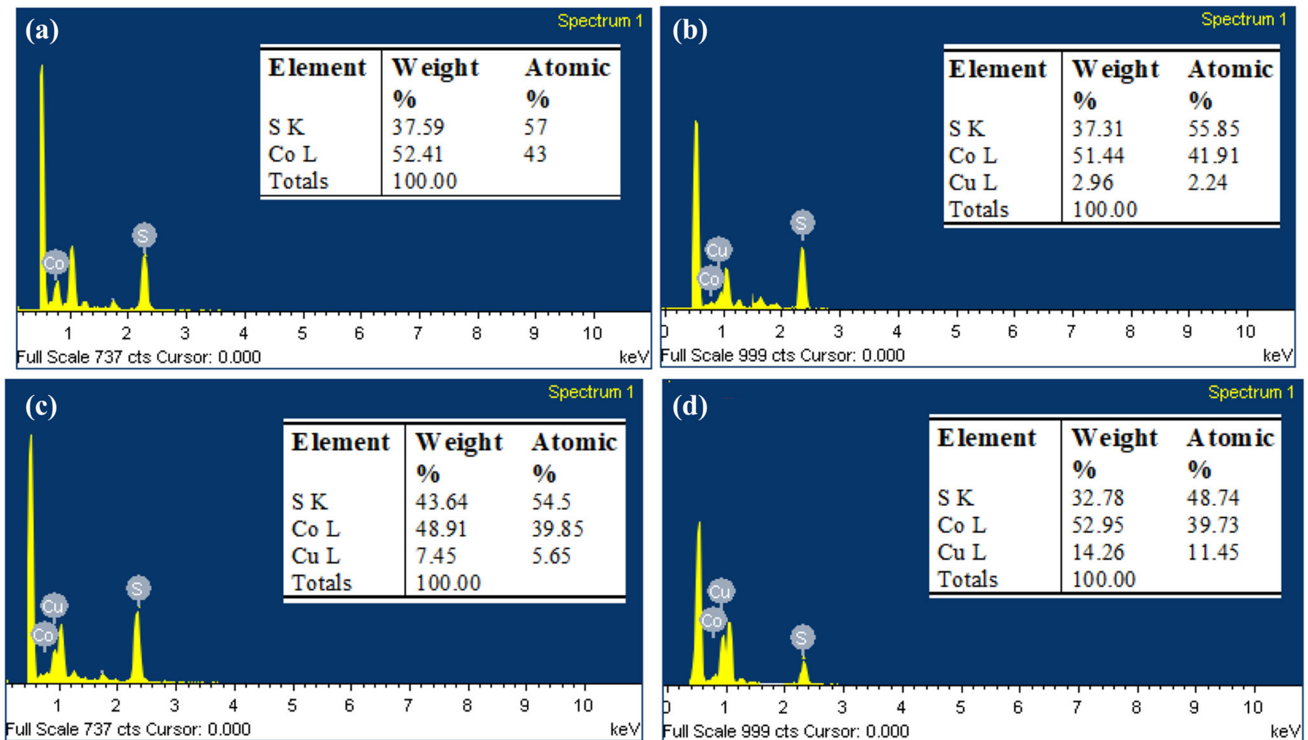

Fig. 4 **a**–**d** EDX analysis of $Cu_xCo_{1-x}S_2$ (x = 0–0.10) thin films

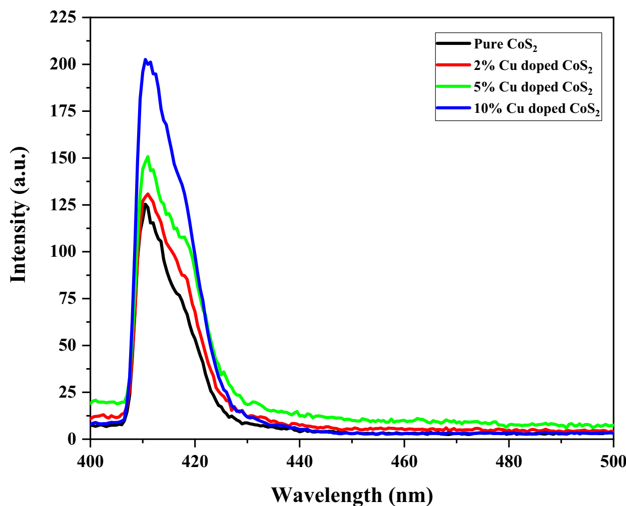

Fig. 5 PL spectra of $Cu_xCo_{1-x}S_2$ (x = 0–0.10) thin films

where A is the area of thin films, t is thin films thickness, ϵ_o is the permittivity of free space, Z' is real impedance, Z'' imaginary impedance and f is the frequency.

Figure 6b illustrates the deviation of dielectric constant and the dielectric loss as a function of frequency at Cu doping concentration. It can be observed that the value of dielectric constant is higher at low frequency for pure and doped thin films and decreased as the frequency because of incompetence of dipole with large deviation of applied electric field. In the present work, it can be observed that as the Cu doping concentration rises the absolute value of dielectric constant increases may be due to more dipole to be directed along the applied field. The dielectric loss of pure CoS_2 is less than that of all doped samples. In general, the dielectric losses happen due to immersion of electrical energy which is employed for revolutions of dipolar molecules [38]. In nanostructure materials, inhomogeneities generate an immersion current due to the space charge creation resultant in a dielectric loss [39].

The a.c conductivity value for pure and Cu-doped CoS_2 thin films was determines using equation given below [40]:

$$\sigma_{ac} = \frac{t}{A} \cdot \frac{Z'}{Z'^2 + Z''^2} \tag{11}$$

Figure 6d depicts the typical plot of $\log(\sigma_{ac})$ versus $\ln(f)$ at different Cu doping concentrations. At low frequencies range, the conductivity is not dependent on the frequency, that could be ascribed due to DC contribution. At high frequency region, it rises with

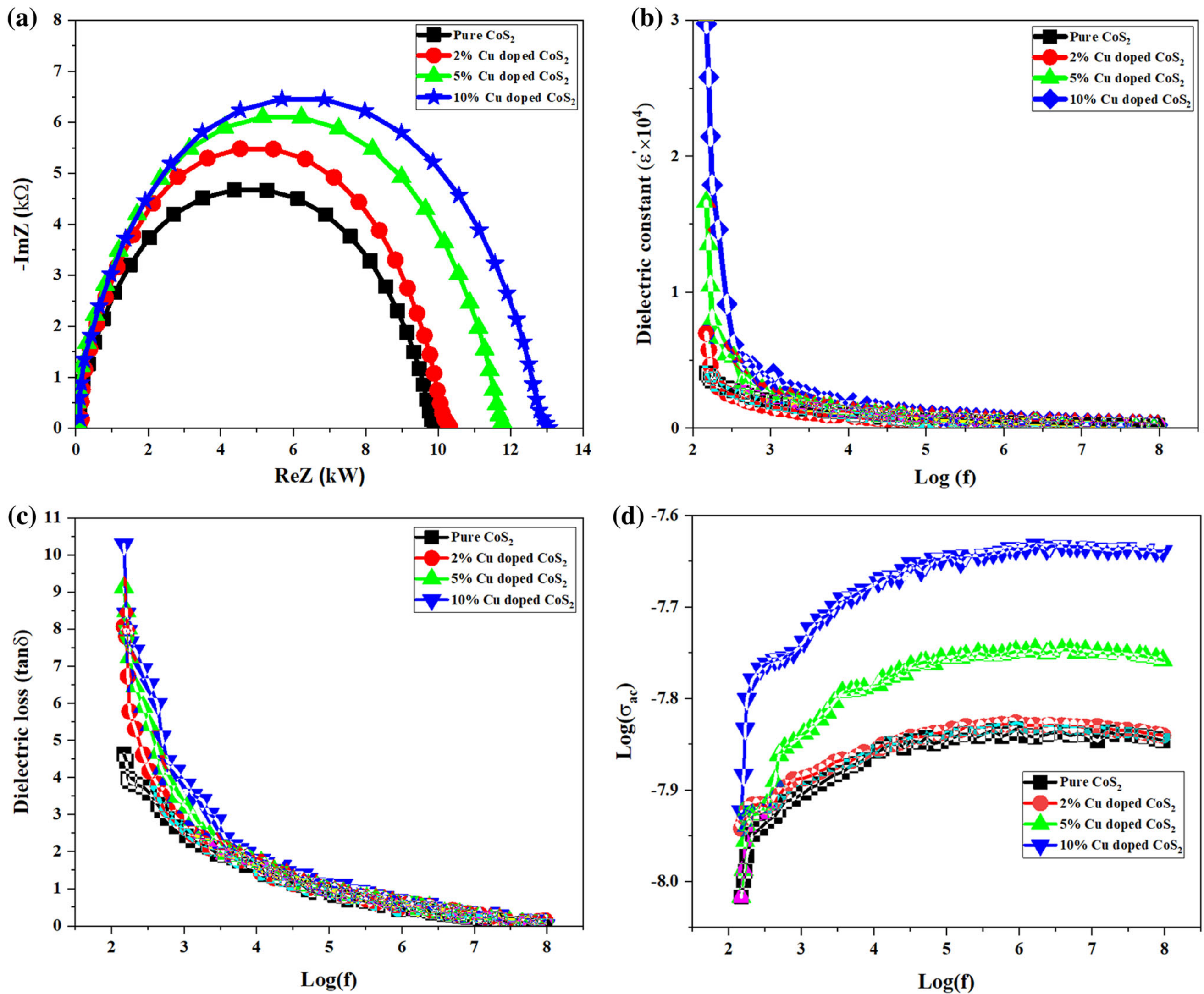

Fig. 6 **a** Nyquist plots and (inset) equivalent circuit, **b** dielectric Constant—log(*f*) plot, **c** dielectric Loss versus log (*f*) and **d** graph of log(σ_{ac} versus log(*f*) of $Cu_xCo_{1-x}S_2$ (x = 0–0.10) thin films by interpretation of impedance analysis

Table 2 Electrical parameters eliminated using impedance spectroscopy

Sample	R_1 (kΩ)	C_1 (pF)
Pure CoS_2	9.64	3.16
2% Cu-doped CoS_2	10.6	3.11
5% Cu-doped CoS_2	11.3	2.95
10% Cu-doped CoS_2	13.1	2.67

frequency. Consequently, the AC conductivity is taken over at high frequencies. It is found that AC conductivity shifts to higher values with Cu doping.

4 Conclusion

We have studied the nanostructural, morphological, photoluminescence and electrical properties of Cu_x-$Co_{1-x}S_2$ (x = 0–0.1) thin films deposited by SILAR technique on glass substrate. It has been found that pure and doped thin films have crystallization in cubic pyrite structural phase of CoS_2 with preferential orientation along (200) direction. The intensity of XRD peaks rises with Cu doping is the indication of enhancement in crystalline. On the other hand, the morphological study showed that the substrate was well covered with spherical grain distribution and grain sizes decreased from 56 to 34 nm with increasing the Cu concentration. The stoichiometry of

all films is confirmed with EDX analysis which was the good agreement with experimental composition. The PL spectra revealed that broad peak modifies and the intensity gradually intensifies by Cu doping level. The results obtained by impedance measurements in terms of the copper content was found that they endorse the effects those found by XRD mainly the structure. The present study has provided us the structural, defects and electrical parameters and motivating for the use of such materials as a counter electrode of solar cells.

Acknowledgements

The authors extend their sincere appreciation to researchers supporting project number (RSP-2020/130), King Saud University, Riyadh, Saudi Arabia for funding this research.

Author contributions

Conceptualization, SMA and SSA; methodology, MSA and SMA; analysis, KS and TU; investigation, SMA and TU; writing-original draft preparation, SMA and MAMK; revision and editing, SMA and JA.

Compliance with ethical standards

Conflict of interest The authors declare that they have no known competing financial interest or personal relationships that could have appeared to influence the work reported in this manuscript.

References

1. D. Kong, J.J. Cha, H. Wang, H.R. Lee, Y. Cui, Energy Environ. Sci. **6**, 3553 (2013)
2. D.S. Kong, H.T. Wang, Z.Y. Lu, Y. Cui, J. Am. Chem. Soc. **136**, 4897 (2014)
3. M.S. Faber, K. Park, M. Cabán-Acevedo, P.K. Santra, S. Jin, J. Phys. Chem. Lett. **4**, 1843 (2013)
4. A. Ivanovskaya, N. Singh, R.F. Liu, H. Kreutzer, J. Baltrusaitis, T.V. Nguyen, H. Metiu, E. McFarland, Langmuir **29**, 480 (2013)
5. T. Thio, J.W. Bennett, Phys. Rev. B **50**, 10574 (1994)
6. M. Cabán-Acevedo, D. Liang, K.S. Chew, J.P. DeGrave, N.S. Kaiser, S. Jin, ACS Nano **9**(7), 1731 (2013)
7. R. Yamamoto, A. Machida, Y. Moritom, A. Nakamura, Phys. B **281**, 705 (2000)
8. H. Yamada, K. Terao, M. Aoki, J. Magn. Magn. Mater. **177**, 607 (1998)
9. T. Shishidou, A.J.R. Freeman Asahi, Phys. Rev. B. **64**, 180401 (2001)
10. P.J. Masset, R.A. Guidotti, J. Power Sources **178**, 456 (2008)
11. J.M. Yan, H.Z. Huang, J. Zhang, Z.J. Liu, Y. Yang, J. Power Sources **145**, 264 (2005)
12. P.V. Kamat, J. Phys. Chem. Lett. **4**, 908 (2013)
13. L. Guo, J. Deng, G. Wang, Y.H. Ke, X. Wang, Y. Yang, Adv. Funct. Mater. **28**, 1804540 (2018)
14. J. Hao, W. Yang, Z. Peng, C. Zhang, Z. Huang, W. Shi, ACS Catal. **7**, 4214–4220 (2017)
15. H.J. Kim, C.W. Kim, D. Punnoose, C.V.V.M. Gopi, S.K. Kim, K. Prabakar, S.S. Rao, Appl. Surf. Sci. **328**, 78–85 (2015)
16. S.K. Shinde, M.B. Jalak, S.Y. Kim, H.M. Yadav, G.S. Ghodake, A.A. Kadam, D.Y. Kim, Ceram. Int. **44**, 23102–23108 (2018)
17. V.P. Deshpande, A.U. Ubale, J. Mater. Sci. **27**, 12826–12833 (2016)
18. X.H. Chen, R. Fan, Chem. Mater. **13**, 802 (2001)
19. X.F. Qian, X.M. Zhang, C. Wang, K.B. Tang, Y. Xie, Y.T. Qian, J. Alloys Compd. **278**, 110 (1998)
20. C.J. Chen, P.T. Chen, M. Basu, K.C. Yang, Y.R. Lu, C.L. Dong, C.G. Ma, C.C. Shen, S.F. Hu, R.S. Liu, J. Mater. Chem. A **3**, 23466 (2015)
21. L. Zhu, D. Susac, M. Teo, K.C. Wong, P.C. Wong, R.R. Parsons, D. Bizzotto, K.A.R. Mitchell, S.A. Campbell, J. Catal. **258**, 235–242 (2008)
22. S. Bausch, B. Sailer, H. Keppner, G. Willeke, E. Bucher, G. Frommeyer, Appl. Phys. Lett. **57**, 25 (1990)
23. J.J. Li, Y.A. Wang, W. Guo, J.C. Keay, T.D. Mishima, M.B. Johnson, X. Peng, J. Am. Chem. Soc. **125**, 12567 (2003)
24. J. Yang, Z. Jin, T. Liu, C. Li, Y. Shi, Sol. Energy Mater. Sol. Cells **92**, 621 (2008)
25. X. Hong, S. Li, X. Tang, Z. Sun, F. Li, J. Alloy. Compd. **749**, 586–593 (2018)
26. M.T.S. Nair, P.K. Nair, R.A. Zingaro, E.A. Meyers, J. Appl. Phys. **74**(3), 1879 (1993)
27. K.C. Preetha, K.V. Murali, A.J. Ragina, K. Deepa, T.L. Remadevi, Curr. Appl. Phys. **12**, 5359 (2012)
28. C.S. Barett, T.B. Massalski, *Crystallographic Methods Principles and Data*, 3rd edn. (McGraw Hill, New York, 1996).
29. M. Shkir, A. Khan, A.M. El-Toni, A. Aldalbahi, I.S. Yahia, S. AlFaify, J. Phys. Chem. Solids **130**, 189–196 (2019)
30. A. Arulanantham, S. Valanarasu, A. Kathalingam, K. Jeyadheepan, J. Mater. Sci. **29**, 11358–11366 (2018)

31. M. Lei, R. Zhang, H.J. Yang, Y.G. Wang, Mater. Lett. **76**, 87–89 (2012)
32. L. Xue, L. Xaing, L.P. Ting, C.X. Wang, L. Ying, C.C. Bao, Chin. Phys. B **19**, 027202 (2010)
33. H.J. Egelhaaf, D. Oelkrug, J. Cryst. Growth **161**, 190–194 (1996)
34. S. Taibl, G. Fafilek, J. Fleig, Nanoscale **8**, 13954–13966 (2016)
35. C.B. Mohmed, K. Karoui, S. Saidi, K. Guidara, A.B. Rhaiem, Phys. B **451**, 87–95 (2014)
36. K.S. Udapa, P.M. Rao, S. Aithal, A.P. Bhat, D.K. Avasthi, Bull. Mater. Sci. **20**, 1069 (1997)
37. M. Shakir, B.K. Singh, R.K. Gaur, B. Kumar, G. Bhagavannarayana, M.A. Wahab, Chalcogenide Lett. **6**, 655 (2009)
38. D. Prabaharan, K. Sadaiyandi, M. Mahendran, S. Sagadevan, Mat. Res. **19**(2), 478–482 (2016)
39. S. Suresh, Syth. Int. J. Phys. Sci. **8**(21), 1121–1127 (2013)
40. A.K. Jonscher, Nature **267**, 673 (1997)

Publisher's Note Springer Nature remains neutral with regard to jurisdictional claims in published maps and institutional affiliations.